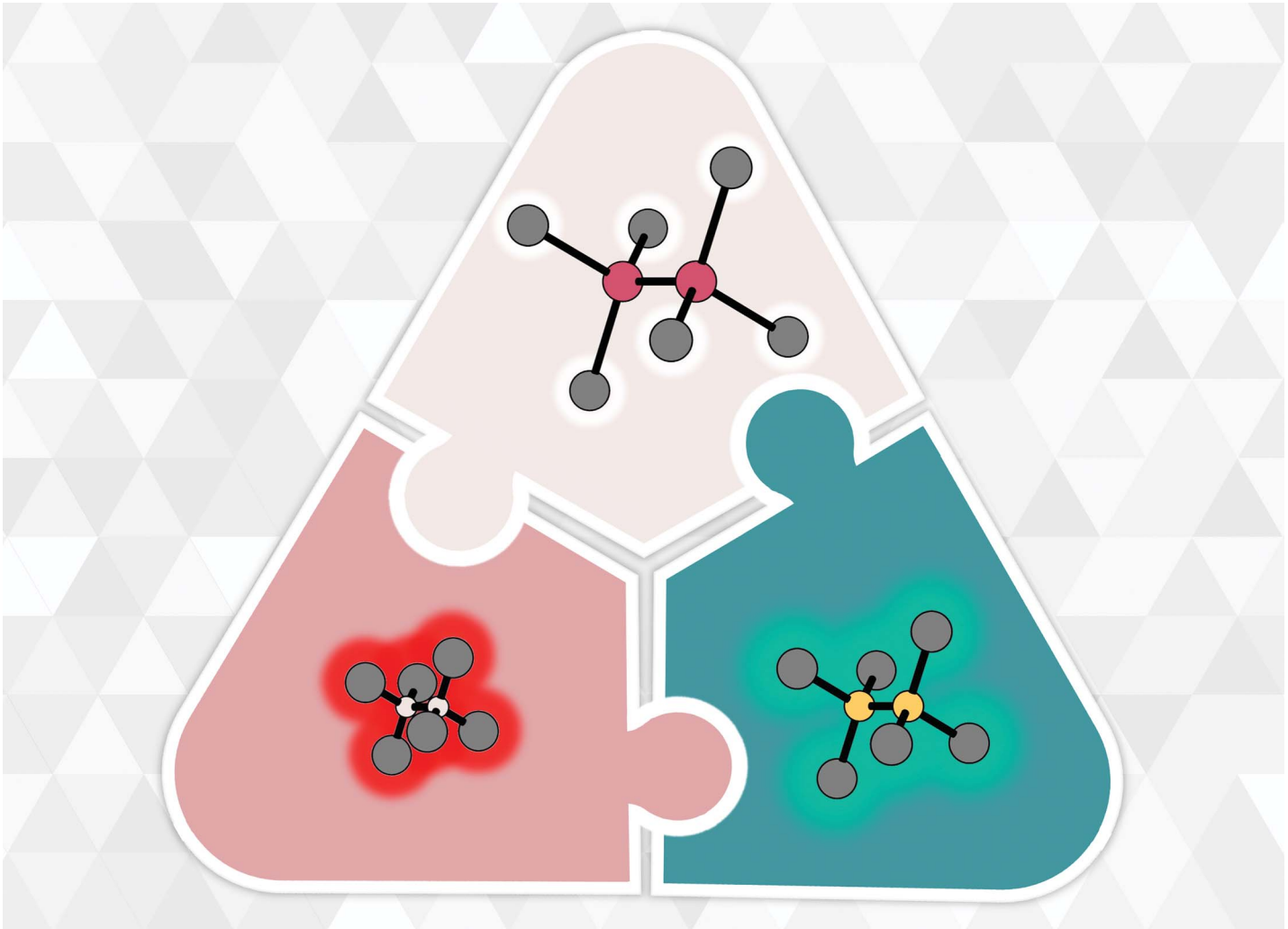

Showcasing research from Professor Bickelhaupt's group, Department of Chemistry and Pharmaceutical Sciences, Vrije Universiteit Amsterdam, The Netherlands.

Nature and strength of group-14 A–A' bonds

A–A' bonds become longer, weaker, and less sensitive to bulky substituents going down group-14 in the periodic table. Systematic increase of steric bulk of the substituents R has opposite effects on $R_3C–CR_3$ and $R_3Si–SiR_3$ bonds: the former becomes weaker, whereas the latter becomes stronger. Bonding analyses show how this different behavior stems from the interplay of (Pauli) repulsive and (dispersion) attractive steric mechanisms. Further increasing the size of the group-14 atoms reduces the sensitivity of the bond strength with respect to the substituents' bulkiness.

As featured in:

See F. Matthias Bickelhaupt *et al.*, *Chem. Sci.*, 2024, **15**, 1648.

ROYAL SOCIETY OF CHEMISTRY

rsc.li/chemical-science

Registered charity number: 207890

Chemical Science

ROYAL SOCIETY OF CHEMISTRY

EDGE ARTICLE

View Article Online
View Journal | View Issue

Check for updates

Cite this: *Chem. Sci.*, 2024, **15**, 1648

All publication charges for this article have been paid for by the Royal Society of Chemistry

Received 20th November 2023
Accepted 7th January 2024

DOI: 10.1039/d3sc06215e

rsc.li/chemical-science

Open Access Article. Published on 16 January 2024. Downloaded on 2/25/2026 9:35:54 AM. This article is licensed under a Creative Commons Attribution 3.0 Unported Licence.

Nature and strength of group-14 A–A′ bonds†

Daniela Rodrigues Silva, ‡[a] Eva Blokker, ‡[a] J. Martijn van der Schuur, [b] Trevor A. Hamlin [a] and F. Matthias Bickelhaupt *[acd]

We have quantum chemically investigated the nature and stability of C–C and Si–Si bonds in $R_3A–AR_3$ (A = C, Si; $R_3 = H_3$, Me_3, Me_2Ph, $MePh_2$, Ph_3, t-Bu_3) using density functional theory (DFT). Systematic increase of steric bulk of the substituents R has opposite effects on C–C and Si–Si bonds: the former becomes weaker whereas the latter becomes stronger. Only upon going further, from R = Ph to the bulkiest R = t-Bu, the $R_3Si–SiR_3$ bond begins to weaken. Our bonding analyses show how different behavior upon increasing the steric bulk of the substituents stems from the interplay of (Pauli) repulsive and (dispersion) attractive steric mechanisms. Extension of our analyses to other model systems shows that C–Si bonds display behavior that is in between that of C–C and Si–Si bonds. Further increasing the size of the group-14 atoms from C–C and Si–Si to Ge–Ge, Sn–Sn and Pb–Pb leads to a further decrease in the sensitivity of the bond strength with respect to the substituents' bulkiness. Our findings can be used as design principles for tuning A–A and A–A′ bond strengths.

Introduction

The carbon atom is not the most abundant element on earth. Yet, it plays a fundamental role in human life as it is the universal connector of organic compounds.[1] The $R_3C–CR_3$ bond is remarkably strong and stable compared to other homodiatomic bonds.[2] Furthermore, its strength can be easily tuned by modulation of the steric properties of the R groups. Thus, the $R_3C–CR_3$ bond is gradually weakened as the number and size of the R groups increase (*e.g.*, from hydrogen to methyl to ethyl to isopropyl).[3] However, if R becomes too bulky, the $R_3C^{\bullet}$ radicals do not dimerize because their mutual steric repulsion becomes too large in which case alternative bonding patterns occur. A remarkable example is the so-called hexaphenylethane ($Ph_3C–CPh_3$) riddle,[4] where two $Ph_3C^{\bullet}$ radicals do not dimerize to form hexaphenylethane, although believed so for many decades.[5] Instead, they form an unsymmetrical quinoid structure (*i.e.*, {[4-(diphenylmethylene)cyclohexa-2,5-dien-1-yl]methane-triyl}tribenzene).[6] Hexaphenylethane became over the years a theoretical construct used as a reference to explore the limits of the C–C bond length and strength.[7] In a series of seminal works,[8] Schreiner and coworkers showed that the C–C bond could be stabilized by increasing steric bulk in the all-*meta-tert*-butyl derivative of hexaphenylethane because of stabilizing dispersion interactions, also referred to as steric attraction.[9]

Silicon is the third-period congener of, and therefore resembles in certain aspects, carbon. At the same time, silicon also exhibits vastly different bonding capacities.[10] For example, silicon can readily form stable hypervalent compounds while carbon does not.[11] Interestingly, contrary to the C–C bond, the Si–Si bond is *strengthened* in hexaphenyldisilane ($Ph_3Si–SiPh_3$) compared to sterically less congested analogs (*e.g.*, $H_3Si–SiH_3$).[12] The origin of this dichotomy has been attributed to common steric and electronic effects.[13] Nevertheless, despite these efforts, the opposite behavior of the C–C *versus* the Si–Si bonds is still incompletely understood and lacks an overarching model that is soundly rooted in quantum mechanics.

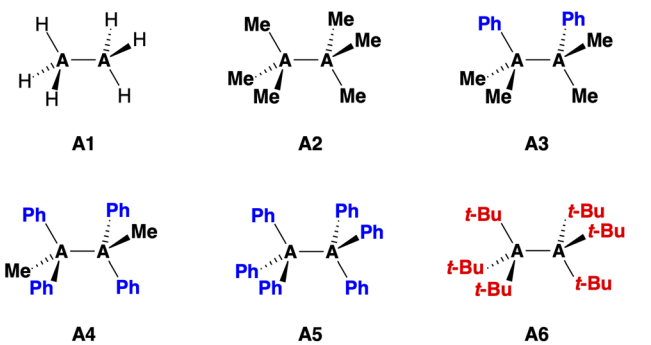

Fig. 1 Model systems $R_3A–AR_3$ for A = C (**C1–6**) and A = Si (**Si1–6**).

[a]*Department of Chemistry and Pharmaceutical Sciences, AIMMS, Vrije Universiteit Amsterdam, De Boelelaan 1108, Amsterdam 1081 HZ, The Netherlands. E-mail: f.m.bickelhaupt@vu.nl; Web: https://www.theochem.nl*

[b]*Polymer Specialties, Nouryon, Zutphenseweg 10, Deventer 7418 AJ, The Netherlands*

[c]*Institute of Molecules and Materials, Radboud University, Heyendaalseweg 135, Nijmegen 6525 AJ, The Netherlands*

[d]*Department of Chemical Sciences, University of Johannesburg, Auckland Park, Johannesburg 2006, South Africa*

† Electronic supplementary information (ESI) available. See DOI: https://doi.org/10.1039/d3sc06215e

‡ These authors contributed equally to this work.

© 2024 The Author(s). Published by the Royal Society of Chemistry

Open Access Article. Published on 16 January 2024. Downloaded on 2/25/2026 9:35:54 AM. This article is licensed under a Creative Commons Attribution 3.0 Unported Licence.

Herein, we investigate the bonding mechanism in the R_3A–AR_3 model systems (A = C, Si; R_3 = H_3, Me_3, Me_2Ph, $MePh_2$, Ph_3, t-Bu_3; see eqn (1) and Fig. 1) as a function of the A–A bond distance using the activation strain model (ASM)[14] in conjunction with Kohn–Sham molecular orbital theory (KS-MO)[15] and a matching energy decomposition analysis (EDA).[16]

$$R_3A^{\bullet} + {}^{\bullet}AR_3 \rightarrow R_3A\text{–}AR_3 \; \Delta H = -\Delta H_{BDE} \quad (1)$$

We wish to understand why the C–C and Si–Si bonds behave differently upon increasing the steric bulk of the substituents. The crux turns out to be the fact that steric (Pauli) repulsion between substituents is a short-range interaction[16a] that is more important in the case of short bonds (*i.e.*, C–C and C–R) whereas steric (dispersion) attraction is a long-range interaction[9] that dominates in the case of longer bonds (Si–Si and Si–R). Indeed, C–Si bonds show behavior with respect to variation in the bulkiness of substituents R which is in between that of C–C and Si–Si bonds. Also, further increasing the size of the group-14 atoms along Ge–Ge, Sn–Sn and Pb–Pb shows an additional attenuation of the sensitivity of the bond strength with respect to the substituents' steric demand. The findings that emerge from our bonding analyses on a systematic set of R_3A–AR_3 model systems can be used as design principles for tuning the strength of A–A and A–A′ bonds.

Computational methods

Computational details

All calculations were performed using the Amsterdam Density Functional (ADF) program (ADF2019.305 for the A–A and constrained R_3A–AR_3 bonding analyses as well as mixed R_3C–SiR_3 and heavier R_3A–AR_3 (A = Ge, Sn, Pb) systems, whereas ADF2017.111 was used for all other computations).[17] Geometries and energies were calculated at the BLYP level of the generalized gradient approximation (GGA).[18] The DFT-D3(BJ) method developed by Grimme and coworkers,[19] which contains the damping function introduced by Becke and Johnson,[20] was used to correct for dispersion interactions. Molecular orbitals (MOs) were expanded using a large, uncontracted set of slater-type orbitals (STO): TZ2P.[21] The TZ2P basis set is of triple-ζ quality, augmented by two sets of polarization functions. All electrons were treated variationally. The trends and conclusions emerging from our BLYP-D3(BJ)/TZ2P computations are nicely reproduced at the M06-2X[22]/TZ2P level (see Table S1 and Fig. S1†). The radical fragments were treated with a spin-unrestricted formalism. The accuracies of the fit scheme (Zlm fit)[23] and the integration grid (Becke grid)[24] were set to EXCELLENT. All geometry optimizations were performed in C_1 symmetry without any symmetry constraint. All optimized structures were confirmed to be true minima (no imaginary frequencies) through vibrational analyses.[25]

Thermochemistry

Bond enthalpies at 298.15 K and 1 atm (ΔH) were calculated from electronic bond energies (ΔE) and vibrational frequencies using standard thermochemistry relations for an ideal gas, according to eqn (2):[26]

$$\Delta H = \Delta E + \Delta E_{trans,298} + \Delta E_{rot,298} + \Delta E_{vib,0} + \Delta(\Delta E_{vib,0})_{298} + \Delta(pV) \quad (2)$$

Here, $\Delta E_{trans,298}$, $\Delta E_{rot,298}$, and $\Delta E_{vib,0}$ are the differences between the reactants (*i.e.*, $R_3A^{\bullet}$, the radical fragments) and product (*i.e.*, R_3A–AR_3, the complex) in translational, rotational, and zero-point vibrational energy, respectively. $\Delta(\Delta E_{vib,0})_{298}$ is the change in the vibrational energy difference as one goes from 0 to 298.15 K. The vibrational energy corrections are based on our frequency calculations. The molar work term $\Delta(pV)$ is $(\Delta n)RT$; $\Delta n = -1$ for two $R_3A^{\bullet}$ radicals combining to one R_3A–AR_3 molecule. Thermal corrections for the electronic energy are neglected.

Activation strain model and energy decomposition analysis

In the activation strain model (ASM),[14] the overall A–A bond energy ΔE [which also features in eqn (2)] between two radicals $R_3A^{\bullet}$ in R_3A–AR_3 is decomposed into two major components:

$$\Delta E = \Delta E_{strain} + \Delta E_{int} \quad (3)$$

Here, the strain energy ΔE_{strain} is the amount of energy required to deform the radical fragments from their equilibrium structure to the geometry that they acquire in the final molecule. The interaction energy ΔE_{int} corresponds to the actual energy change when the geometrically deformed $R_3A^{\bullet}$ fragments are combined to form R_3A–AR_3.

We further analyze the interaction energy ΔE_{int} within the framework of the Kohn–Sham molecular orbital (KS-MO)[15] model by dissecting it using our canonical energy decomposition analysis (EDA)[16] scheme into electrostatic interactions, Pauli repulsion, (attractive) orbital interactions, dispersion corrections, and spin polarization:

$$\Delta E_{int} = \Delta V_{elstat} + \Delta E_{Pauli} + \Delta E_{oi} + \Delta E_{disp} + \Delta E_{spinpol} \quad (4)$$

The electrostatic energy ΔV_{elstat} corresponds to the electrostatic interactions between the unperturbed charge distribution of the radical fragments $R_3A^{\bullet}$, which is usually attractive. The Pauli repulsion ΔE_{Pauli} comprises the destabilizing interactions between occupied orbitals and is responsible for any steric repulsion. The orbital interactions ΔE_{oi} term accounts for electron-pair bonding (the SOMO–SOMO interaction), charge transfer (donor–acceptor interaction between an occupied orbital of one fragment with an empty orbital of the other fragment), and polarization (empty/occupied orbital mixing on one fragment due to the presence of another fragment). The dispersion energy ΔE_{disp} is added as a correction.[19] Finally, the $\Delta E_{spinpol}$ term refers to the spin polarization of the spin-α and spin-β electrons of the deformed unrestricted fragments and is with respect to ΔE_{int} destabilizing (*i.e.*, the deformed unrestricted fragments without spin polarization lie consistently 2–4 kcal mol^{-1} higher in energy and therefore have a too stabilizing ΔE_{int}; see Table S2†).[27] The open-shell PyFrag2019 program was used to analyze the bond dissociation as a function of the R_3A–AR_3 distance.[28]

Open Access Article. Published on 16 January 2024. Downloaded on 2/25/2026 9:35:54 AM. This article is licensed under a Creative Commons Attribution 3.0 Unported Licence.

Results and discussion

General trends in bond strength

The bond enthalpies ΔH [eqn (1)] under standard conditions (298.15 K and 1 atm) of the $R_3A–AR_3$ model systems (A = C, Si; $R_3 = H_3$, Me_3, Me_2Ph, $MePh_2$, Ph_3, t-Bu_3) from our BLYP-D3(BJ)/TZ2P computations are collected in Table 1. The computed trends in ΔH, and hence in bond strength, agree very well with available experimental data (see Table S3†).[29] We find that the Si–Si bond in **Si1** is intrinsically weaker and longer than the C–C bond in **C1** ($\Delta H = -71.4$ kcal mol^{-1} and $r_{Si–Si} = 2.356$ Å for **Si1** and $\Delta H = -85.2$ kcal mol^{-1} and $r_{C–C} = 1.538$ Å for **C1**). Furthermore, the $R_3C–CR_3$ bond systematically weakens and elongates as the R groups are varied from hydrogen to methyl to phenyl, for example, from −85.2 kcal mol^{-1} and 1.538 Å for **C1** to −4.6 kcal mol^{-1} and 1.738 Å for **C5**. The opposite trend emerges for $R_3Si–SiR_3$ along the same R series, that is, the Si–Si bond becomes slightly stronger from −71.4 kcal mol^{-1} for **Si1** to −78.5 kcal mol^{-1} for **Si5**. The Si–Si bond length varies little and is *ca.* 2.36 Å in all cases. Only with the addition of the isotropically bulky *tert*-butyl group[30] in **Si6**, the Si–Si bond does significantly weaken and stretch ($\Delta H = -41.0$ kcal mol^{-1} and $r_{Si–Si} = 2.726$ Å).[31] The *t*-Bu groups in **C6** encumber the dimerization of the t-$Bu_3C^{\bullet}$ radicals,[32] which are known as persistent radicals.[33]

The electronic bond energy ΔE is slightly more stabilizing than the ΔH, mainly due to zero-point vibrational energy effects in the latter, and always retains the same overall trends as the latter (Table 1). Therefore, to understand the origin of the aforementioned trends in C–C and Si–Si bond strengths, we analyze the features in the bonding mechanism that determine the trends in ΔE using the activation strain model (ASM),[14] which decomposes ΔE into the strain energy ΔE_{strain} and the interaction energy ΔE_{int} (eqn (3); see Computational methods for a theoretical overview). Inspection of the ASM terms in Table 1 reveals that, in all cases, the trends in bond strength ΔE emerge from the trends in the interaction energy ΔE_{int}. For example, the Si–Si bond in **Si1** is weaker than the C–C bond in **C1** ($\Delta E = -74.3$ kcal mol^{-1} and −92.1 kcal mol^{-1}, respectively) because of a less stabilizing interaction between $H_3Si^{\bullet}$ radicals than between $H_3C^{\bullet}$ radicals ($\Delta E_{int} = -74.8$ kcal mol^{-1} for **Si1** and −110.4 kcal mol^{-1} for **C1**). The weakening of the C–C bond from **C1** to **C5** ($\Delta E = -92.1$ kcal mol^{-1} and −7.0 kcal mol^{-1}, respectively) and strengthening of the Si–Si bond from **Si1** to **Si5** ($\Delta E = -74.3$ kcal mol^{-1} and −79.8 kcal mol^{-1}, respectively) also comes from the interaction energy that becomes less and more stabilizing, respectively ($\Delta E_{int} = -110.4$ kcal mol^{-1} for **C1** and −72.2 kcal mol^{-1} for **C5**, whereas $\Delta E_{int} = -74.8$ kcal mol^{-1} for **Si1** and −81.0 kcal mol^{-1} for **Si5**). Furthermore, the C–C bond strength is also determined by strain energy ΔE_{strain}. As will be discussed later, part of the less stabilizing ΔE_{int} is absorbed into a more destabilizing ΔE_{strain}, which is associated with the pyramidalization of the $R_3A^{\bullet}$ radicals upon formation of the $R_3A–AR_3$ bond. Below, we systematically elucidate each of these features and provide their underlying physical mechanism.

Table 1 Bond enthalpies (ΔH; in kcal mol^{-1}), activation strain model terms (in kcal mol^{-1}), and bond lengths (in Å) of the $R_3A–AR_3$ bonds (A = C, Si; $R_3 = H_3$, Me_3, Me_2Ph, $MePh_2$, Ph_3, t-Bu_3)[a]

No.	Species[b]	ΔH	ΔE	ΔE_{strain}	ΔE_{int}	$r_{A–A}$
C1	$H_3C–CH_3$	−85.2	−92.1	18.4	−110.4	1.538
C2	$Me_3C–CMe_3$	−64.0	−69.6	25.0	−94.6	1.597
C3[c]	$PhMe_2C–CMe_2Ph$	−42.1	−46.8	39.7	−86.5	1.627
C4[d]	$Ph_2MeC–CMePh_2$	−25.9	−29.9	56.9	−86.8	1.638
C5	$Ph_3C–CPh_3$	−4.6	−7.0	65.1	−72.2	1.738
Si1	$H_3Si–SiH_3$	−71.4	−74.3	0.6	−74.8	2.356
Si2	$Me_3Si–SiMe_3$	−73.0	−75.1	0.3	−75.4	2.357
Si3[c]	$PhMe_2Si–SiMe_2Ph$	−73.8	−74.7	0.7	−75.4	2.356
Si4[d]	$Ph_2MeSi–SiMePh_2$	−74.4	−75.3	3.5	−78.8	2.353
Si5	$Ph_3Si–SiPh_3$	−78.5	−79.8	1.2	−81.0	2.358
Si6	t-$Bu_3Si–Si$$t$-$Bu_3$	−41.0	−45.8	15.0	−60.8	2.726

[a] Computed at BLYP-D3(BJ)/TZ2P at 298.15 K and 1 atm. All structures are staggered (for more details, see Table S4). [b] **C6** does not form a stable C–C electron-pair bond. [c] *Gauche* conformation. [d] *Anti* conformation.

Intrinsic bond strength

Before examining the effect of substituents, we wish to understand the difference in the intrinsic strength between the C–C and Si–Si bonds in the unsubstituted, archetypal model systems ethane **C1** and disilane **Si1**. Why is the Si–Si bond in **Si1** weaker than the C–C bond in **C1**, *i.e.*, why is ΔE less stabilizing for the former than for the latter? To facilitate an equitable comparison of the studied systems to arrive at the actual causalities in their bonding mechanism, our bonding analyses are carried out as a function of the A–A bond distance from now on (Fig. 2). As will become clear in the following, our analyses reveal that the Si–Si bond in **Si1** is weaker than the C–C bond in **C1** due to the increase in effective atom size of Si compared to C and, thus, the increase in Pauli repulsion. This pushes the distance between the two Si atoms to a longer value and also weakens the bond compared to two C atoms. The bond weakening from C–C to Si–Si occurs despite an electron-pair bond that, at most bond distances, becomes stronger, not weaker, because of a larger bonding overlap between the spatially more extended (and diffuse) silyl SOMOs compared to the more compact methyl SOMOs. This is reminiscent of the weakening and lengthening of C–X bonds as X is varied from F to I.[34]

As can be seen in Fig. 2, the trends in the interaction energy ΔE_{int} determine the trends in bond energy ΔE and cause the Si–Si bond to be weaker than the C–C bond. Therefore, we further analyze the bonding mechanism and the interaction energy ΔE_{int} using quantitative Kohn–Sham MO theory[15] and a matching canonical energy decomposition analysis (EDA),[16] which dissects ΔE_{int} into the electrostatic interactions ΔV_{elstat}, Pauli repulsion ΔE_{Pauli}, and orbital interactions ΔE_{oi}, among others (eqn (4); see Computational methods for a theoretical overview). Our quantitative MO and EDA analyses reveal a key role for the Pauli repulsion ΔE_{Pauli} behind the weaker Si–Si than C–C bond. In both cases, the main factor preventing the two atoms from coming closer than the equilibrium distance is Pauli repulsion between occupied closed-shell orbitals. The spatially more extended valence AOs of Si lead to the occurrence of a larger

© 2024 The Author(s). Published by the Royal Society of Chemistry

Open Access Article. Published on 16 January 2024. Downloaded on 2/25/2026 9:35:54 AM.
This article is licensed under a Creative Commons Attribution 3.0 Unported Licence.

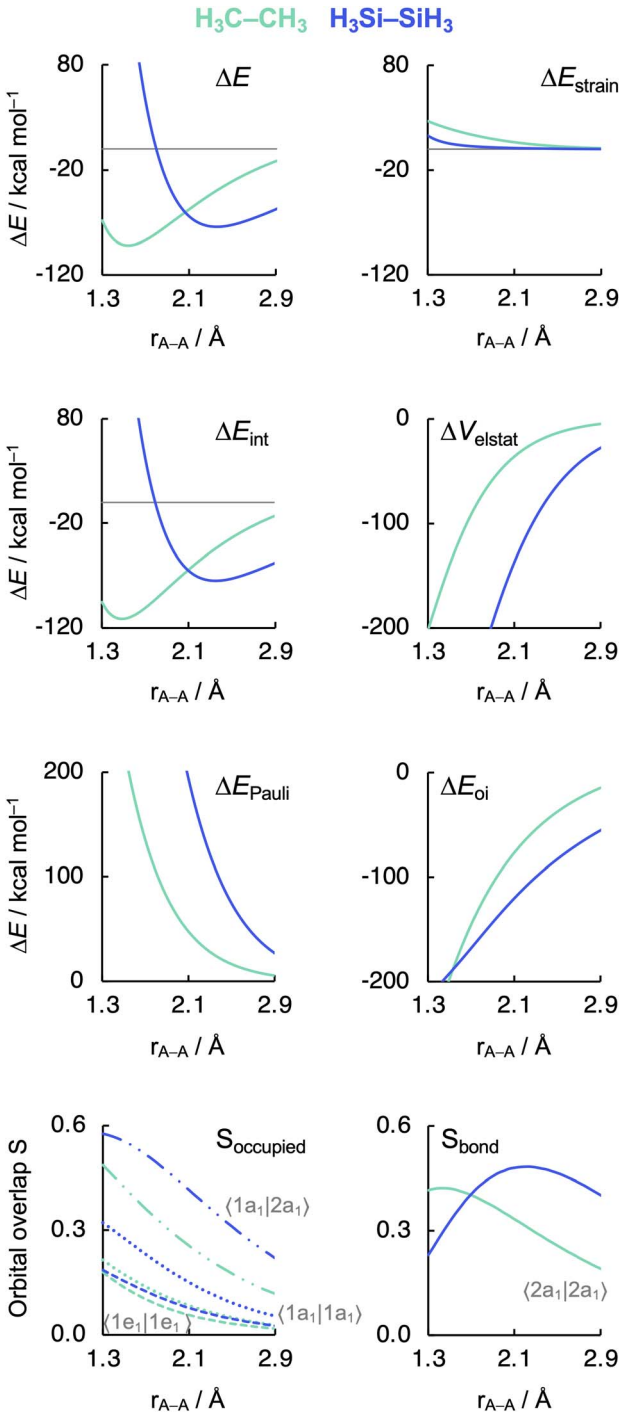

Fig. 2 Energy decomposition analysis terms, main occupied–occupied orbital overlaps ($S_{occupied}$), and SOMO–SOMO overlap (S_{bond}) as a function of the A–A distance in H_3A–AH_3 (**1**, A = C, Si). The dispersion energy ΔE_{disp} is nearly constant and, therefore, not shown. See Fig. 3 for the schematic $AH_3^{\bullet}$ FMOs. Computed at BLYP-D3(BJ)/TZ2P. MO numbering starts at the lowest-energy valence AO combination.

occupied–occupied orbital overlap at a longer A–A distance than in the case of the more compact valence AOs of C ($S_{occupied}$, see Fig. 2). In addition, Si has a larger number of closed-shell subvalence orbitals (Fig. 3). This situation gives rise to more ΔE_{Pauli} for Si–Si than for C–C, which pushes the Si–Si bond to a longer equilibrium distance, where all energy terms are weaker. Note that ΔE_{Pauli} is partially absorbed into the destabilizing strain energy ΔE_{strain}.[35] The $H_3A^{\bullet}$ radicals pyramidalize to reduce the build-up of steric Pauli repulsion between the substituents as the A–A distance becomes shorter (see Fig. S2 and Table S5†). The ΔE_{strain} is always less destabilizing for **Si1** than **C1** because $H_3Si^{\bullet}$ is already pyramidal in its equilibrium geometry, while $H_3C^{\bullet}$ needs to pyramidalize from its planar equilibrium geometry upon formation of the C–C bond.[36]

Both electrostatic and orbital interactions (ΔV_{elstat} and ΔE_{oi}, respectively) are more stabilizing for **Si1** than for **C1**, thus counteracting, but not overruling, the trends set by ΔE_{Pauli}. The Si atom has a large nuclear charge and electron cloud, which leads to a stronger electrostatic attraction between the electrons of one $H_3Si^{\bullet}$ fragment with the nuclei of the other $H_3Si^{\bullet}$ fragment than between two $H_3C^{\bullet}$ fragments, at any given bond distance.[37] Furthermore, the spatially more extended valence AOs of Si lead to an earlier buildup of SOMO–SOMO bond overlap (S_{bond}) as the two fragments are approaching (see Fig. 2 and 3), although the cancelation of overlap also begins earlier. This situation results in a more stabilizing ΔE_{oi} for **Si1** than **C1** at longer A–A distances. The stabilization of ΔE_{oi} upon shortening the A–A distance below the optimum electron-pair bond overlap S_{bond} is due to other donor–acceptor orbital interactions (see Fig. S3†). The earlier onset of cancellation effects on the Si–Si bond overlap causes a shallower slope in the ΔE_{oi} curve of the Si–Si bond, which therefore comes closer to, and crosses, the ΔE_{oi} curve of the C–C bond which remains steeper at these short distances.

Interestingly, the maximum value of the S_{bond} overlap is also larger for Si than C (S_{bond} = 0.48 and 0.42, respectively). This effect can be traced back to the $\langle np_z|np_z\rangle$ overlap between the bare A–A atoms (A = C, Si; Fig. 4). Note that, at the A–A distance with maximum $\langle np_z|np_z\rangle$ (*i.e.*, 1.8 Å and 2.5 Å for C–C and Si–Si, respectively), the C $2p_z$ orbital crosses the nodal surface and begins to enter into an out-of-phase admixture with the rear lobe of the other C $2p_z$ orbital (see red counter lines of the $np_z \cdot np_z$ overlap densities in Fig. 4). This cancellation of overlap does not occur to the same extent for Si as the radial node of the Si $3p_z$ orbital (nonexistent in C $2p_z$) pushes the region of maximum amplitude of the $3p_z$ lobe further away from the Si nucleus. This circumstance delays the out-of-phase overlap with the backside lobe of the $3p_z$ AO of the other Si atom, resulting in a larger maximum $\langle np_z|np_z\rangle$ overlap and, therefore, a larger S_{bond} for the Si–Si bond than for the C–C bond. The trend from the C–C to the Si–Si bond continues for the heavier group-14 elements with increasingly larger maximum bond overlaps $\langle np_z|np_z\rangle$ at increasingly longer A–A distances going down group 14 from A = C and Si to Ge, Sn, and Pb (see Fig. S4 and S5†). The largest increase in maximum bond-overlap values, however, occurs in the step from period 2 to period 3 where, for the first time along the series, a p-core shell is introduced. Finally, note that the maximum S_{bond} occurs at a H_3A–AH_3 bond distance (A = C, Si) slightly shorter than the corresponding equilibrium bond length (Fig. 2). Again, it is the increasing Pauli repulsion at

© 2024 The Author(s). Published by the Royal Society of Chemistry

Open Access Article. Published on 16 January 2024. Downloaded on 2/25/2026 9:35:54 AM.
This article is licensed under a Creative Commons Attribution 3.0 Unported Licence.

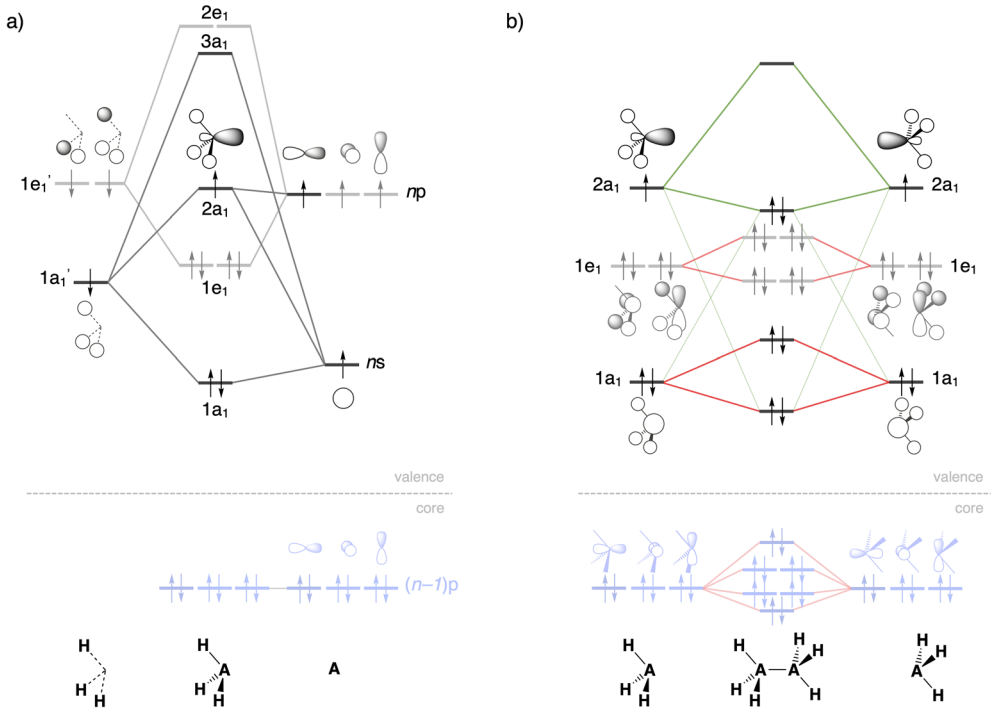

Fig. 3 Schematic molecular orbital diagrams of (a) pyramidal $H_3A^{\bullet}$ and (b) $H_3A–AH_3$ (A = C, Si). Core Si 2p orbitals are highlighted in light blue, A–A electron-pair bond and donor–acceptor interactions in green, occupied–occupied orbital repulsion in red. MO numbering starts at the lowest-energy valence AO combination.

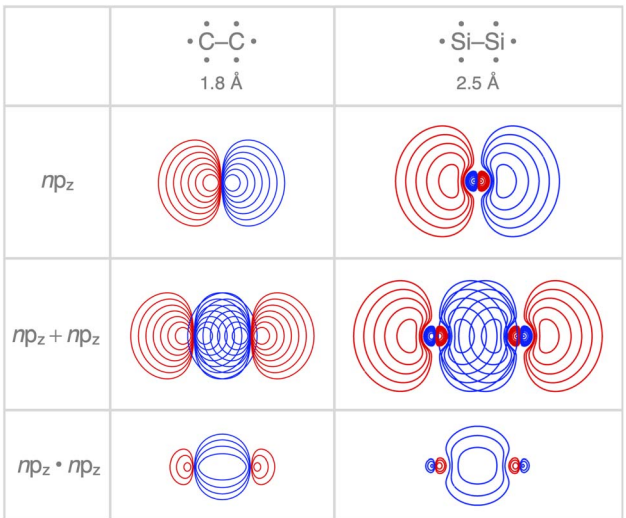

Fig. 4 Contour plots (10 contour lines between 0.03, 1.0 for np_z and $np_z + np_z$, and between 0.003, 1.0 for $np_z \cdot np_z$; color represents phase) of the carbon and silicon np_z atomic orbitals, their maximum overlap, and respective $np_z \cdot np_z$ overlap density in A–A (A = C, Si). Atoms in their sp^3 atomic configuration, computed at BLYP-D3(BJ)/TZ2P.

shorter distances that pushes the equilibrium bond lengths to a longer $H_3A–AH_3$ distance. Altogether, our findings once more highlight the well-known role of the Pauli repulsive orbital interactions in determining the length and strength of main-group element bonds.[34,37b,38]

Effect of steric hindrance

Now that we understand the difference in intrinsic $R_3C–CR_3$ and $R_3Si–SiR_3$ ($R_3 = H_3$) bonding mechanism, we evaluate the effect of changing the steric size of the R groups. All trends change systematically on going from $R_3 = H_3$ to *t*-Bu_3. Hence, we focus our discussion mainly on $R_3 = H_3$ and Ph_3 to pinpoint the origin of the opposite trends, that is, of decreasing C–C bond strength going from **C1** to **C5** and increasing Si–Si bond strength going from **Si1** to **Si5**. As will become clear in the following, these opposite trends arise from the net steric interactions that are destabilizing for C (*i.e.*, steric repulsion) and stabilizing for Si (*i.e.*, steric attraction) because of the different A–R bond lengths (A = C, Si) and, consequently, R···R distances. Thus, if the R groups are in closer proximity, as in the C systems, due to the shorter C–C and C–R bond lengths, the interaction energy is dominated by the steric Pauli repulsion term, which causes a weakening of the C–C bond as R increases in size. On the other hand, when the R groups are farther apart from each other, as in the Si systems, due to the intrinsically longer Si–Si and Si–R bonds, the steric repulsion is smaller and becomes dominated by steric attraction, resulting in an overall more stabilizing interaction energy and, therefore, Si–Si bond strengthening from $R_3 = H_3$ to Ph_3. Our findings support and extend earlier reports in the literature that discuss the interplay of repulsive and attractive steric effects in determining the length and strength of C–C bonds and other pheonomena.[8,30]

The ASM and EDA terms as a function of the A–A distance for the $R_3A–AR_3$ systems (A = C, Si; $R_3 = H_3$, Ph_3) are given in Fig. 5 (see Fig. S6–S8† for the complete data set). As can be seen in

© 2024 The Author(s). Published by the Royal Society of Chemistry

Open Access Article. Published on 16 January 2024. Downloaded on 2/25/2026 9:35:54 AM.
This article is licensed under a Creative Commons Attribution 3.0 Unported Licence.

Fig. 5, the opposite trends, for $R_3Si–SiR_3$ compared to $R_3C–CR_3$, in bond strength ΔE going from $R_3 = H_3$ to Ph_3 originates mainly from the interaction energy ΔE_{int}. That is, from $R_3 = H_3$ to Ph_3, ΔE_{int} becomes less stabilizing for C–C (*i.e.*, from full to dashed green lines) and more stabilizing for Si–Si (*i.e.*, from full to dashed blue lines). The substitution of the H atoms by Ph groups in $R_3A–AR_3$ results in an increase in steric Pauli repulsion between the $R_3A^\bullet$ fragments. As R increases in size, the number of occupied–occupied orbital overlaps also increases, resulting in a larger ΔE_{Pauli}. As mentioned before, part of ΔE_{Pauli} is absorbed into the strain energy ΔE_{strain} as the $R_3A^\bullet$ fragments deform in response to the increasing steric repulsion (Fig. 5; see also Fig. S2 and Table S5†). In $R_3C–CR_3$, the R groups are in closer proximity due to the short C–R bonds and, therefore, this increase in steric repulsion is large enough to cause a weakening of the C–C bond going from **C1** to **C5** (Fig. 6). This effect is much less pronounced in $R_3Si–SiR_3$ simply because the R groups are farther removed from each other compared to $R_3C–CR_3$ (the Si–R bonds are longer than the C–R bonds; Fig. 6). If the C–C bond is artificially placed in the Si–Si geometry and *vice versa*, we observe that the trends in the interaction energy are reversed (Fig. S9†). That is, as R is varied from H to Ph, ΔE_{int} becomes more stabilizing for C and less stabilizing for Si.

The much less pronounced increase in Pauli repulsion ΔE_{Pauli} going from $R_3 = H_3$ to Ph_3 in $R_3Si–SiR_3$ allows for the long-range, weakly stabilizing interactions (see ΔV_{elstat} and ΔE_{disp} in Fig. 5), also referred to as steric attraction,[9] to take over and strengthen the Si–Si bond from **Si1** to **Si5**. The ΔV_{elstat} term is dominated by the nuclear–electron electrostatic attraction,[37] which becomes more stabilizing as R increases in size. The same occurs for the dispersion energy ΔE_{disp} as larger substituent surfaces are in each other's proximity, close enough for dispersion interaction but not yet having large mutual closed-shell overlap. The only exception is the isotropically bulky *tert*-butyl group (*i.e.*, $R_3 = t\text{-}Bu_3$), whose mutual closed-shell overlap and thus steric Pauli repulsion is large enough to cause a weakening even of the Si–Si bond (Fig. S7†).

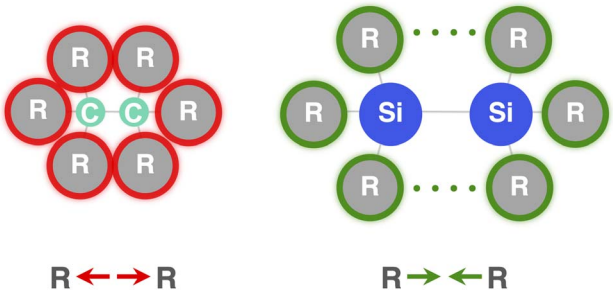

Fig. 6 The C–C bond is short and easily weakened by steric Pauli repulsion between bulkier substituents. The Si–Si bond is long and at first benefits from steric dispersion attraction between bulkier substituents.

Generalization

Finally, we evaluate the generality of the steric effects observed in the $R_3A–AR_3$ (A = C, Si; $R_3 = H_3$, Me_3, Me_2Ph, $MePh_2$, Ph_3, $t\text{-}Bu_3$) model systems by extending our bonding analysis to mixed $R_3C–SiR_3$ ($R_3 = H_3$, Ph_3, $t\text{-}Bu_3$) and heavier $R_3A–AR_3$ (A = Ge, Sn, Pb; $R_3 = H_3$, Ph_3, $t\text{-}Bu_3$) systems. As can be seen in Fig. 7 (the complete dataset is provided in Table S6†), the C–Si bond shows behavior in between that of the C–C and the Si–Si bonds while still retaining the C–C bond sensitivity to steric hindrance. The $H_3C–SiH_3$ bond is somewhat weaker and longer (ΔH = −83.2 kcal mol^{-1} and $r_{C–Si}$ = 1.888 Å) than $H_3C–CH_3$ (ΔH = −85.2 kcal mol^{-1} and $r_{C–C}$ = 1.538 Å) while stronger and shorter than $H_3Si–SiH_3$ (ΔH = −71.4 kcal mol^{-1} and $r_{Si–Si}$ = 2.356 Å). This is again due to the increase in mutual steric Pauli repulsion between the radical fragment as one $H_3A^\bullet$ is varied from $H_3C^\bullet$ to $H_3Si^\bullet$ (Fig. S10†).

On the other hand, the sensibility of the $R_3A–AR_3$ bond strength towards the substituents' bulkiness decreases as the central atom increases in size from C–C and Si–Si to Ge–Ge, Sn–Sn, and Pb–Pb (see Table S7† the complete dataset). Note that

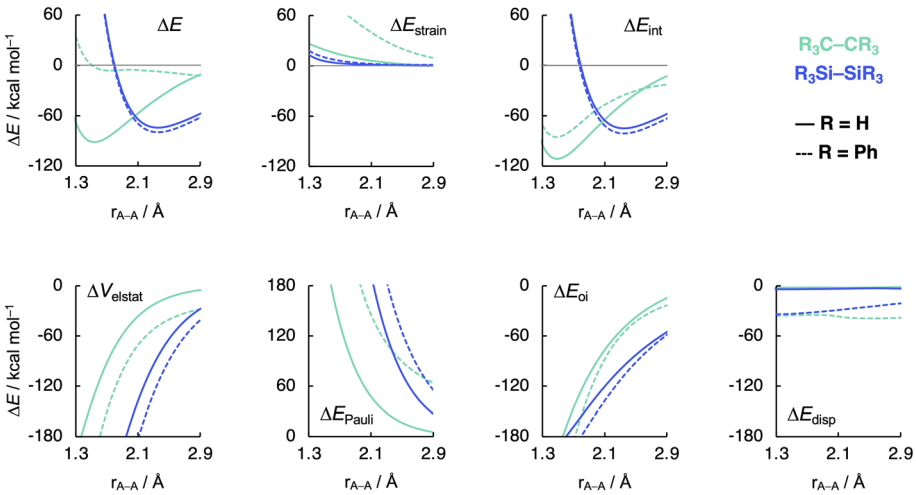

Fig. 5 Activation strain model (top row) and energy decomposition analysis (bottom row) as a function of the A–A distance in $R_3A–AR_3$ (A = C, Si; $R_3 = H_3$, Ph_3) computed at BLYP-D3(BJ)/TZ2P.

Open Access Article. Published on 16 January 2024. Downloaded on 2/25/2026 9:35:54 AM. This article is licensed under a Creative Commons Attribution 3.0 Unported Licence.

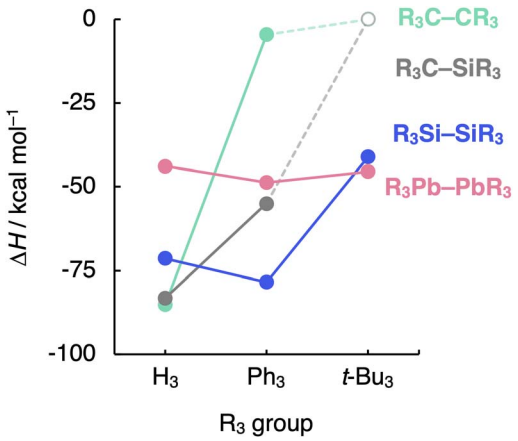

Fig. 7 Bond enthalpies (ΔH) of the R_3A–AR_3 (A = C, Si, Pb; R_3 = H_3, Ph_3, t-Bu_3) systems computed at BLYP-D3(BJ)/TZ2P for A = C, Si and at ZORA-BLYP-D3(BJ)/TZ2P for A = Pb.

the R_3Pb–PbR_3 bond weakens by *ca.* 3 kcal mol^{-1} as R_3 is varied from H_3 to t-Bu_3, while the R_3Si–SiR_3 bond weakens by almost 30 kcal mol^{-1} (Fig. 7). This is again due to the increase in the effective atom size of A and, therefore, the longer R···R distances. If the R groups are packed together, as in R_3C–CR_3, occupied–occupied orbital overlap is significant and the R_3A–AR_3 bond strength is dominated by steric repulsion between the substituents. If the R groups are further away from each other, as in R_3Si–SiR_3 and heavier analogs, that overlap becomes negligible, and dispersion takes over; thus, steric repulsion turns into steric attraction. But if the A–A and A–R bond becomes too long and, therefore, the R groups are too far removed from each other, both short-range repulsive and long-range attractive steric effects are weakened (see ASM and EDA terms in Fig. S11 and S12†), and the R_3A–AR_3 bond is almost insensitive to the size of R. The latter holds in particular for the Pb–Pb bond (see Fig. 7).

Conclusions

The Si–Si bond is intrinsically longer, weaker, and much less sensitive to substitution of H substituents for bulkier groups than the C–C bond. Thus, whereas the R_3C–CR_3 bond significantly weakens as R is varied from H to Me to Ph, the R_3Si–SiR_3 bond is somewhat strengthened along the same R series and only weakens when R is the isotropically bulky t-Bu group. This follows from our quantum chemical bonding analyses using dispersion-corrected density functional theory.

The H_3Si–SiH_3 bond is longer and weaker than the H_3C–CH_3 bond because the larger number of occupied shells and the larger spatial extension of silicon's valence AOs cause an earlier onset of, and a stronger, steric Pauli repulsion that destabilizes the Si–Si bond and pushes it to a longer equilibrium distance. This trend and mechanism hold for the entire series of group-14 H_3A–AH_3 bonds which become weaker and longer along C–C, Si–Si, Ge–Ge, Sn–Sn, and Pb–Pb. Interestingly, this is so despite the electron-pair bonding overlap and orbital interactions becoming stronger, not weaker, along this series. The reason for the increasing bond overlap is the introduction of a radial node in the valence np_z orbital from C to Si, which delays the occurrence of cancellation of bond overlap between the SOMOs, resulting in a larger maximum SOMO–SOMO overlap for Si.

When the hydrogen atoms in H_3C–CH_3 are replaced by larger R groups, the C–C bond is weakened due to a steep increase in steric Pauli repulsion between the R groups which is partially converted into strain energy associated with geometrical deformation of the R_3C moieties in R_3C–CR_3. This increase in steric repulsion is less pronounced in R_3Si–SiR_3 as the R groups are farther removed from each other due to the longer Si–R bonds. Then, repulsive interactions are compensated by long-range attractive ones in R_3Si–SiR_3. Only R = t-Bu gives rise to steric repulsion that is large enough to cause a weakening of the R_3Si–SiR_3 bond. The sensitivity of the bond strength with respect to the substituents' bulkiness (even for R = t-Bu) further decreases going down group-14 due to the increasingly longer A–R bonds. Our findings nicely equip chemists with the rational design principles to tune the strength of A–A and A–A′ bonds at will.

Data availability

All data of this study are available in the main text and ESI.†

Author contributions

FMB and JMS conceived the project, which was supervised by TAH and FMB. DRS and EB carried out the quantum chemical computations and bonding analyses. DRS also drafted the manuscript. DRS, TAH, and FMB discussed all results. All authors reviewed the manuscript.

Conflicts of interest

There are no conflicts of interest to declare.

Acknowledgements

This work is part of the Advanced Research Center for Chemical Building Blocks (ARC CBBC; grant 2018.019.B), which is co-founded and co-financed by the Dutch Research Council (NWO) and the Netherlands Ministry of Economic Affairs and Climate Policy. This work was carried out on the Dutch national e-infrastructure with the support of SURF Cooperative. Furthermore, we thank Dr Lucas de Azevedo Santos and Dr Pascal Vermeeren for helpful discussions.

References

1 J. Clayden, N. Greeves and S. G. Warren, *Organic Chemistry*, Oxford University Press, Oxford, 2012.
2 Y.-R. Luo, *Comprehensive Handbook of Chemical Bond Energies*, CRC Press, Boca Raton, 2007.
3 C. Rüchardt and H.-D. Beckhaus, *Angew. Chem., Int. Ed.*, 1980, **19**, 429; *Angew. Chem.*, 1980, **92**, 417.

© 2024 The Author(s). Published by the Royal Society of Chemistry

Open Access Article. Published on 16 January 2024. Downloaded on 2/25/2026 9:35:54 AM. This article is licensed under a Creative Commons Attribution 3.0 Unported Licence.

4 J. M. McBride, *Tetrahedron*, 1974, **30**, 2009, and references cited therein.
5 M. Gomberg, *J. Am. Chem. Soc.*, 1900, **22**, 757.
6 (*a*) H. Lankamp, W. T. Nauta and C. MacLean, *Tetrahedron Lett.*, 1968, **9**, 249; (*b*) P. Jacobsen, *Ber. Dtsch. Chem. Ges.*, 1905, **38**, 196.
7 (*a*) S. Grimme and P. R. Schreiner, *Angew. Chem., Int. Ed.*, 2011, **50**, 12639; *Angew. Chem.*, 2011, **123**, 12849; (*b*) Y. Uchimura, T. Takeda, R. Katoono, K. Fujiwara and T. Suzuki, *Angew. Chem., Int. Ed.*, 2015, **54**, 4010; *Angew. Chem.*, 2015, **127**, 4082; (*c*) S. Rösel, C. Balestrieri and P. R. Schreiner, *Chem. Sci.*, 2017, **8**, 405; (*d*) E. Dames, B. Sirjean and H. Wang, *J. Phys. Chem. A*, 2010, **114**, 1161.
8 (*a*) P. R. Schreiner, L. V. Chernish, P. A. Gunchenko, E. Yu. Tikhonchuk, H. Hausmann, M. Serafin, S. Schlecht, J. E. P. Dahl, R. M. K. Carlson and A. A. Fokin, *Nature*, 2011, **477**, 308; (*b*) J. P. Wagner and P. R. Schreiner, *Angew. Chem., Int. Ed.*, 2015, **54**, 12274; *Angew. Chem.*, 2015, **127**, 12446; (*c*) S. Rösel, J. Becker, W. D. Allen and P. R. Schreiner, *J. Am. Chem. Soc.*, 2018, **140**, 14421; (*d*) E. Solel, M. Ruth and P. R. Schreiner, *J. Org. Chem.*, 2021, **86**, 7701.
9 (*a*) R. Hoffmann, C. C. Levin and R. A. Moss, *J. Am. Chem. Soc.*, 1973, **95**, 629; (*b*) R. R. Sauers, *J. Chem. Educ.*, 1996, **73**, 114.
10 (*a*) M. Karni, Y. Apeloig, J. Kapp and P. von R. Schleyer, in *The Chemistry of Organic Silicon Compounds*, ed. Z. Rappoport and Y. Apeloig, John Wiley & Sons, 2001, pp. 1–163; (*b*) Y. Apeloig, in *The Chemistry of Organic Silicon Compounds*, ed. S. Patai and Z. Rappoport, John Wiley & Sons, 1989, pp. 57–225.
11 S. C. A. H. Pierrefixe, C. Fonseca Guerra and F. M. Bickelhaupt, *Chem.–Eur. J.*, 2008, **14**, 819.
12 (*a*) L. M. Calle and A. S Kana'an, *J. Chem. Thermodyn.*, 1974, **6**, 935; (*b*) J. M. Gaidis, P. R. Briggs and T. W. Shannon, *J. Phys. Chem.*, 1971, **75**, 974; (*c*) H. Gilman, R. K. Ingham and A. G. Smith, *J. Org. Chem.*, 1953, **18**, 1743; (*d*) H. Gilman and T. C. Wu, *J. Am. Chem. Soc.*, 1951, **73**, 4031.
13 (*a*) B. Tumanskii, M. Karni and Y. Apeloig, in *Organosilicon Compounds: Theory and Experiment (Synthesis)*, ed. V. Ya. Lee, Elsevier, 2017, pp. 231–294; (*b*) C. Rüchardt and H.-D. Beckhaus, Synthetic organic chemistry, in *Topics in Current Chemistry*, Springer, Berlin, Heidelberg, 1980, vol. 130, pp. 1–22.
14 (*a*) P. Vermeeren, T. A. Hamlin and F. M. Bickelhaupt, *Chem. Commun.*, 2021, **57**, 5880; (*b*) P. Vermeeren, S. C. C. van der Lubbe, C. Fonseca Guerra, F. M. Bickelhaupt and T. A. Hamlin, *Nat. Protoc.*, 2020, **15**, 649; (*c*) F. M. Bickelhaupt and K. N. Houk, *Angew. Chem., Int. Ed.*, 2017, **56**, 10070; *Angew. Chem.*, 2017, **129**, 10204; (*d*) L. P. Wolters and F. M. Bickelhaupt, *Wiley Interdiscip. Rev.: Comput. Mol. Sci.*, 2015, **5**, 324; (*e*) I. Fernández and F. M. Bickelhaupt, *Chem. Soc. Rev.*, 2014, **43**, 4953; (*f*) W.-J. van Zeist and F. M. Bickelhaupt, *Org. Biomol. Chem.*, 2010, **8**, 3118; (*g*) F. M. Bickelhaupt, *J. Comput. Chem.*, 1999, **20**, 114.
15 (*a*) R. van Meer, O. V. Gritsenko and E. J. Baerends, *J. Chem. Theory Comput.*, 2014, **10**, 4432; (*b*) T. A. Albright, J. K. Burdett and W. H. Wangbo, *Orbital Interactions in Chemistry*, Wiley, New York, 2013.
16 (*a*) T. A. Hamlin, P. Vermeeren, C. Fonseca Guerra and F. M. Bickelhaupt, in *Complementary Bonding Analysis*, ed. S. Grabowsky, De Gruyter, Berlin, 2021, pp. 199–212; (*b*) F. M. Bickelhaupt and E. J. Baerends, in *Reviews in Computational Chemistry*, ed. K. B. Lipkowitz and D. B. Boyd, Wiley–VCH, Hoboken, 2000, pp. 1–86.
17 (*a*) *ADF2017.111/2019.305, SCM, Theoretical Chemistry*, Vrije Universiteit Amsterdam, The Netherlands, **http://www.scm.com**; (*b*) G. te Velde, F. M. Bickelhaupt, E. J. Baerends, C. Fonseca Guerra, S. J. A. van Gisbergen, J. G. Snijders and T. Ziegler, *J. Comput. Chem.*, 2001, **22**, 931; (*c*) C. Fonseca Guerra, J. G. Snijders, G. te Velde and E. J. Baerends, *Theor. Chem. Acc.*, 1998, **99**, 391.
18 (*a*) A. D. Becke, *Phys. Rev. A*, 1988, **38**, 3098; (*b*) C. T. Lee, W. T. Yang and R. G. Parr, *Phys. Rev. B: Condens. Matter Mater. Phys.*, 1988, **37**, 785.
19 (*a*) S. Grimme, J. Antony, S. Ehrlich and H. Krieg, *J. Chem. Phys.*, 2010, **132**, 154104; (*b*) S. Grimme, S. Ehrlich and L. Goerigk, *J. Comput. Chem.*, 2011, **32**, 1456.
20 E. R. Johnson and A. D. Becke, *J. Chem. Phys.*, 2005, **123**, 024101.
21 E. van Lenthe and E. J. Baerends, *J. Comput. Chem.*, 2003, **24**, 1142.
22 Y. Zhao and D. G. Truhlar, *Theor. Chem. Acc.*, 2008, **120**, 215.
23 M. Franchini, P. H. T. Philipsen, E. van Lenthe and L. Visscher, *J. Chem. Theory Comput.*, 2014, **10**, 1994.
24 M. Franchini, P. H. T. Philipsen and L. Visscher, *J. Comput. Chem.*, 2013, **34**, 1819.
25 (*a*) A. Bérces, R. M. Dickson, L. Fan, H. Jacobsen, D. Swerhone and T. Ziegler, *Comput. Phys. Commun.*, 1997, **100**, 247; (*b*) H. Jacobsen, A. Bérces, D. P. Swerhone and T. Ziegler, *Comput. Phys. Commun.*, 1997, **100**, 263; (*c*) S. K. Wolff, *Int. J. Quantum Chem.*, 2005, **104**, 645.
26 (*a*) P. W. Atkins and J. de Paula, *Physical Chemistry*, W. H. Freeman, New York, 9th edn, 2010; (*b*) F. Jensen, *Introduction to Computational Chemistry*, Wiley, 2007.
27 F. M. Bickelhaupt, M. Solà and C. Fonseca Guerra, *Faraday Discuss.*, 2007, **135**, 451.
28 (*a*) W. J. van Zeist, C. Fonseca Guerra and F. M. Bickelhaupt, *J. Comp. Chem.*, 2008, **29**, 312; (*b*) X. Sun, T. M. Soini, J. Poater, T. A. Hamlin and F. M. Bickelhaupt, *J. Comput. Chem.*, 2019, **40**, 2227; (*c*) X. Sun, T. Soini, L. P. Wolters, W.-J. van Zeist, C. Fonseca Guerra, T. A. Hamlin and F. M. Bickelhaupt, *PyFrag 2019*, Vrije Universiteit Amsterdam, The Netherlands.
29 A comparison between the ΔH_{BDE} at BLYP-D3(BJ)/TZ2P computed herein with experimental data is provided in Table S3 of the ESI.† See, for example:(*a*) M. Szwarc, *Proc. R. Soc. Lond. A*, 1951, **207**, 5; (*b*) R. Walsh, *Acc. Chem. Res.*, 1981, **14**, 246.
30 L. P. Wolters, R. Koekkoek and F. M. Bickelhaupt, *ACS Catal.*, 2015, **5**, 5766.

© 2024 The Author(s). Published by the Royal Society of Chemistry

Open Access Article. Published on 16 January 2024. Downloaded on 2/25/2026 9:35:54 AM.
This article is licensed under a Creative Commons Attribution 3.0 Unported Licence.

31 The Si–Si bond in **Si6** is known to be unusually long (r_{Si-Si} = 2.687 Å by X-ray data). See: N. Wiberg, H. Schuster, A. Simon and K. Peters, *Angew. Chem., Int. Ed.*, 1986, **25**, 79; *Angew. Chem.*, 1986, **98**, 100.

32 **C6** does not form a stable C–C electron-pair bond. See Table S4 in the ESI.†

33 D. Griller and K. U. Ingold, *Acc. Chem. Res.*, 1976, **9**, 13.

34 E. Blokker, X. Sun, J. Poater, J. M. van der Schuur, T. A. Hamlin and F. M. Bickelhaupt, *Chem.–Eur. J.*, 2021, **27**, 15616.

35 (*a*) E. Blokker, W.-J. van Zeist, X. Sun, J. Poater, J. M. van der Schuur, T. A. Hamlin and F. M. Bickelhaupt, *Angew. Chem., Int. Ed.*, 2022, **61**, e202207477; *Angew. Chem.*, 2022, **134**, e202207477; (*b*) W.-J. van Zeist and F. M. Bickelhaupt, *Phys. Chem. Chem. Phys.*, 2009, **11**, 10317.

36 The methyl radical fragment is planar to minimize steric repulsion between the hydrogen substituents. See:F. M. Bickelhaupt, T. Ziegler and P. von Ragué Schleyer, *Organometallics*, 1996, **15**, 1477.

37 For a detailed discussion on the behavior of ΔV_{elstat} along the formation of a chemical bond, see:(*a*) G. Frenking and F. M. Bickelhaupt, in *The Chemical Bond: Fundamental Aspects of Chemical Bonding*, ed. G. Frenking and S. Shaik, Wiley-VCH, Weinheim, 2014, pp. 121–158; (*b*) A. Krapp, F. M. Bickelhaupt and G. Frenking, *Chem.–Eur. J.*, 2006, **12**, 9196.

38 (*a*) P. Vermeeren, W.-J. van Zeist, T. A. Hamlin, C. Fonseca Guerra and F. M. Bickelhaupt, *Chem.–Eur. J.*, 2021, **27**, 7074; (*b*) F. M. Bickelhaupt, R. L. DeKock and E. J. Baerends, *J. Am. Chem. Soc.*, 2002, **124**, 1500.

© 2024 The Author(s). Published by the Royal Society of Chemistry